ACS APPLIED MATERIALS & INTERFACES

Kinetics and Structural Changes of Li-Rich Layered Oxide $0.5Li_2MnO_3 \cdot 0.5LiNi_{0.292}Co_{0.375}Mn_{0.333}O_2$ Material Investigated by a Novel Technique Combining in Situ XRD and a Multipotential Step

Chong-Heng Shen, Ling Huang,* Zhou Lin, Shou-Yu Shen, Qin Wang, Hang Su, Fang Fu, and Xiao-Mei Zheng

Department of Chemistry, College of Chemistry and Chemical Engineering, Xiamen University, Xiamen, Fujian 361005, China

S *Supporting Information*

ABSTRACT: Li-rich layered oxide $0.5Li_2MnO_3 \cdot 0.5LiNi_{0.292}Co_{0.375}Mn_{0.333}O_2$ was prepared by an aqueous solution−evaporation route. X-ray powder diffraction (XRD) showed that the as-synthesized material was a solid solution consisting of layered α-$NaFeO_2$-type $LiMO_2$ (M = Ni, Co, Mn) and monoclinic Li_2MnO_3. The superlattice spots in the selected area electron diffraction pattern indicated the ordering of lithium ions with transition metal (TM) ions in TM layers in this Li-rich layered oxide. Electrochemical performance testing showed that the as-synthesized material could deliver an initial discharge capacity of 267.7 mAh/g, with a capacity retention of 88.5% after 33 cycles. A new combination technique, multipotential step in situ XRD (MPS in situ XRD) measurement, was applied for the first time to investigate the Li-rich layered oxide. Using this approach, the relationships between kinetics and structural variations can be obtained simutaneously. In situ XRD results showed that the *c* parameter decreased from 3.70 to 4.30 V and increased from 4.30 to 4.70 V, whereas the *a* parameter underwent a decrease above 4.30 V during the first charge process. Below 3.90 V during the first discharge process, a slight decrease in the *c* parameter was found along with an increase in the *a* parameter. During the first charge process, the value of the coefficient of diffusion for lithium ions (D_{Li+}) decreased to its mininum at 4.55 V, which might be associated with Ni^{2+} migration, as indicated by both Ni occupancy in 3b sites (Ni_{3b}%) in the Li^+ layers and complicated chemical reactions. Remarkably, a lattice distortion might occur within the local domain in the host stucture during the first discharge process, indicated by a slight splitting of the (003) diffraction peak at 3.20 V.

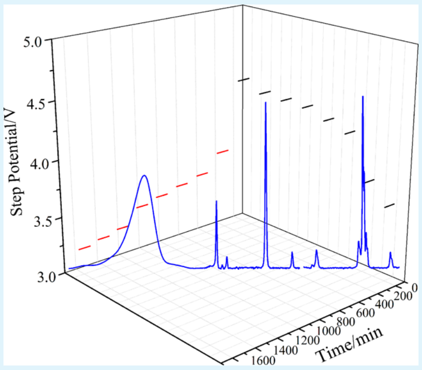

KEYWORDS: *Li-rich layered oxide, multipotential step, in situ XRD, lithium diffusion, Ni migration*

1. INTRODUCTION

The urgent plight related to factors including the economy, population, global warming, and exhausted fossil fuels is inspiring interest in developing advanced and clean power sources.[1−3] Moreover, the rapid development of electric mobility for large-scale applications (such as electric vehicles (EVs), hybrid electric vehicles (HEVs), and plug-in hybrid electric vehicles (PHEVs)), modern information technology for portable electronics, and intermittent renewable energy sources has increased the demand for high-energy-density storage devices.[4−7] In the realm of energy storage, lithium-ion batteries have attracted extensive interest as a clean and advanced power source due to their high energy and power densities, low cost of maintenance, long cycle life, and environmental friendliness.[2,8] Layered $LiCoO_2$ is a promising cathode with respect to its high energy and power densities. However, layered $LiCoO_2$ is not suitable for large-scale EV/PHEV applications due to its limited practical capacity (~140 mAh g^{-1}), chemical and structural instabilities at deep charge stages, high cost, and poor availability.[6,9] To replace $LiCoO_2$, researchers have developed three possible candidates: spinel-type $LiMn_2O_4$ (including its derivatives), olivine-type $LiFePO_4$, and α-$NaFeO_2$ $LiMn_{1/3}Ni_{1/3}Co_{1/3}O_2$. Neverthless, these are also limited by their practical capacity (<200 mAh g^{-1}).[3,10]

In this respect, solid solutions between Li_2MnO_3 and $LiMO_2$ (M = Ni, Co, Mn) have been reported to deliver a very high discharge capacity of over 250 mAh·g^{-1}, to possess an energy density of about 1000 W h kg^{-1}, to be lower cost, and to demonstrate improved safety at elevated temperatures compared to that of traditional cathodes.[11−16] The high capacity of Li-rich layered oxide has been attributed to the electrochemical activation of the Li_2MnO_3 component above 4.40 V during the initial charge process.[17] At 4.50 V, an obvious voltage plateau can be observed, where oxygen loss and removal of the Li_2O component accompany the extraction of Li from the Li_2MnO_3 phase.[18] Despite its outstanding advantages, there are several intrinsic defects in Li-rich layered oxide that hinder its extensive commercial application: its high irreversible

Received: May 20, 2014
Accepted: July 15, 2014
Published: July 15, 2014

dx.doi.org/10.1021/am503132t | *ACS Appl. Mater. Interfaces* 2014, 6, 13271−13279

capacity loss during the initial cycle (low initial Coulombic efficiency) due to the extraction of lithium as Li_2O during the first charge process, its inability to insert all of the lithium ions into the lattice during the discharge process, its shortened voltage plateau, its poor rate capability (caused by the slow kinetics of oxygen diffusion and electron and lithium-ion transport), its voltage fade (attributed to continuous structural transition), and its insufficient capacity retention (large capacity loss during subsequent discharge).[1,5,7−10,13,19,20]

Because most of these drawbacks are associated with the initial charge/discharge process, many advanced observation techniques are aimed at the structural changes and variations in transition metal valence states with respect to Li-rich layered oxide or Li_2MnO_3 during the first cycle. With the aid of in situ hard X-ray absorption near-edge structure (in situ XANES) analysis at the transition metal K-edges and ex situ soft XANES at the oxygen K-edge and transition metal L-edges, Oishi et al. found that Ni^{2+} and Co^{3+} ions are completely oxidized to Ni^{4+} and Co^{4+}, whereas Mn^{4+} remains unchanged and ligand oxygen ions participate in charge compensation in the process of charging to 4.80 V via the plateau voltage region in a $Li_{1.16}Ni_{0.15}Co_{0.19}Mn_{0.50}O_2$ positive electrode material.[16] However, according to Gu et al., evidence of a decrease of the Mn valence state on the surface/grain-boundary down to 2.2+ (compared to 4+ in the bulk crystal) was found by means of a combination of aberration-corrected scanning transmission electron microscopy (STEM), X-ray energy-dispersive spectroscopy (XEDS), electron energy loss spectroscopy (EELS), and complementary multislice image simulation in pristine $Li_{1.2}Ni_{0.2}Mn_{0.6}O_2$.[5] Zheng et al. have reported that a sponge-like structure and fragmented pieces were found on the surface of a layered composite cathode after extended cycling and that formation of Mn^{2+} species with decreased Li content in the fragments leads to a significant capacity loss during cycling using STEM and EELS.[6] Through electrochemical measurements combined with ex situ X-ray absorption (XAS), Croy et al. indicated that the hysteresis in $x Li_2MnO_3 \cdot (1-x) LiMO_2$ is attributed primarily to an inherent structural reorganization after the electrochemical activation of the Li_2MnO_3 component that changes the crystallographic site energies.[17] Yabuuchi et al. found that simultaneous oxygen and lithium removal via the voltage plateau region during the initial charge process leads to structural rearrangement, including a cation migration process from metal to lithium layers in $Li_2MnO_3-LiCo_{1/3}Ni_{1/3}Mn_{1/3}O_2$, through the use of synchrotron X-ray diffraction (SXRD) and XAS.[10] By means of in situ X-ray diffraction (in situ XRD), Mohanty et al. found that the *c* lattice parameter increases during the process of initial charging and finally decreases during the charge process beyond 4.40 V, whereas the *a* lattice parameter remains constant during the first cycle's voltage plateau region for a $Li_{1.2}Co_{0.1}Mn_{0.55}Ni_{0.15}O_2$ cathode, indicating oxygen loss from the structure during the course of initial charging.[21] Combining in situ XRD and ex-TEM, Shen et al. reported the exsistence of a β-MnO_2 phase appearing near 4.54 V in the first charge process and a phase transformation from this phase to layered $Li_{0.9}MnO_2$ occurring during the initial discharge process.[22] Yu et al. confirmed that, in Li_2MnO_3, Mn valence remains the same during the first charge process and is reduced during the discharge process (using ex situ XANES) and that the generation of O_2 occurs during the charge process (using gas chromatography, GC).[23]

Besides the structural changes for the first cycle, the kinetics process, such as lithium ion diffusion and Ni ion migration, is important for studying Li-rich layered oxide. Using galvanostatic intermittent titration (GITT) and electrochemical impedance spectroscopy (EIS), Li et al. indicated that the lithium ion diffusion coefficients (D_{Li+}) during the first charge process were as small as 10^{-19} cm^2 s^{-1} for a $Li[Li_{0.23}Co_{0.3}Mn_{0.47}]O_2$ cathode due to the high kinetic barriers bound up with the concurrent Li^+ extraction, oxygen loss, and structural rearrangement.[24] However, according to Amalraj et al., the measured effective chemical diffusion coefficient of lithium ions in $x Li_2MnO_3 \cdot (1-x) LiMO_2$ during the first charge process to 4.70 V by potentiostatic intermittent titration (PITT) was found to be $\sim 10^{-10}$ cm^2 s^{-1}.[25] Combining convergent beam electron diffraction with Raman spectroscopy studies, they also found that partial structural transformation from layered-type to spinel-type ordering in $x Li_2MnO_3 \cdot (1-x) LiMO_2$ electrodes occurred during the initial charge process to 4.70 V and even at the early states of the charge process at 4.10−4.40 V.[25]

There have been many reports on the structural changes and the kinetics process for Li-rich layered oxide. Neverthless, most of them have been focused on either structural changes or the kinetic process through isolated measurement. Currently, simultaneous measurements that include both structural changes and the kinetic process as well as the relationship between the two have been seldom reported. In this article, we developed a technique that combines multipotential step and in situ XRD (MPS in situ XRD) to simultaneously examine, for the first time, structural changes and kinetics of Li-rich layered oxide during the first charge−discharge process. Different evidence consisting of the value of D_{Li+}, the occupancy of 3b sites in Li^+ layers by Ni (Ni_{3b}%), the full width at half maxmiun (fwhm), and the lattice parameters was obtained. The results could help to explain the impact of structural and phase changes on Ni ion migration and lithium ion diffusion. This MPS in situ XRD measurement was operated in an electrolytic cell device with an electrochemical workstation and X-ray diffractometer.

2. EXPERIMENTAL SECTION

2.1. Synthesis of $0.5Li_2MnO_3 \cdot 0.5LiNi_{0.292}Co_{0.375}Mn_{0.333}O_2$ Material. The precursor was prepared by an aqueous solution−evaporation route.[22] Solution A (1 M) was prepared by mixing $LiAc \cdot 2H_2O$ and $Mn(Ac)_2 \cdot 4H_2O$ at a stoichiometric mole ratio of Li/Mn = 2:1. Solution B (1 M) contained $LiAc \cdot 2H_2O$, $Ni(Ac)_2 \cdot 2H_2O$, $Co(Ac)_2 \cdot 2H_2O$, and $Mn(Ac)_2 \cdot 4H_2O$ at ratio of Li/Ni/Co/Mn = 1:0.292:0.375:0.333. Solution B was placed in a water bath, and solution A was added dropwise. The obtained precursor was burnt to ash. $0.5Li_2MnO_3 \cdot 0.5LiNi_{0.292}Co_{0.375}Mn_{0.333}O_2$ was obtained by heating the ash in air at 900 °C for 12 h followed by a quenching process.

2.2. Charge−Discharge Test and Structural Characterization of $0.5Li_2MnO_3 \cdot 0.5LiNi_{0.292}Co_{0.375}Mn_{0.333}O_2$ Material. The slurry was prepared by mixing $0.5Li_2MnO_3 \cdot 0.5LiNi_{0.292}Co_{0.375}Mn_{0.333}O_2$ with acetylene black and PVDF (8:1:1 by weight). The cathode was prepared by casting the slurry onto Al foil and drying overnight. The charge−discharge test was carried out in a 2025 coin cell including the as-prepared cathode with Li foil as the anode and a 2400 Celgard separator. A 1 M $LiPF_6$ in EC/DMC (3:7 by volume) solution was employed as the electrolyte. X-ray powder diffraction was used to characterize the material's structure using a Rigaku Ultima IV powder diffractometer with Cu Kα radiation (λ = 1.5418 Å). A Hitachi S4800 SEM was used to observe the morphology of the as-prepared material. TEM was conducted with a JEM2100.

2.3. MPS in Situ XRD Experiment. The MPS in situ XRD experiment was conducted with a Rigaku Ultima IV-CHI660D coupling system using an electrolytic cell device consisting of a copper base and an aluminum upper cover with a sealed Kapton film.

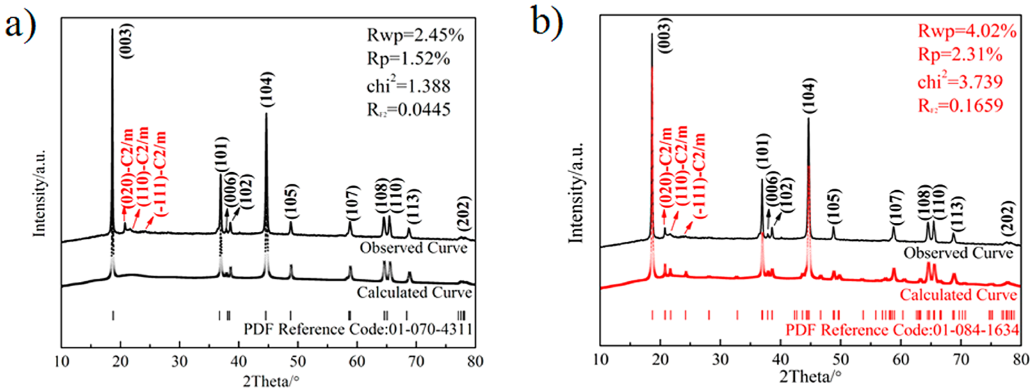

Figure 1. Observed and calculated XRD patterns based on $LiMO_2$ (a) and Li_2MnO_3 (b) of $0.5Li_2MnO_3 \cdot 0.5LiNi_{0.292}Co_{0.375}Mn_{0.333}O_2$.

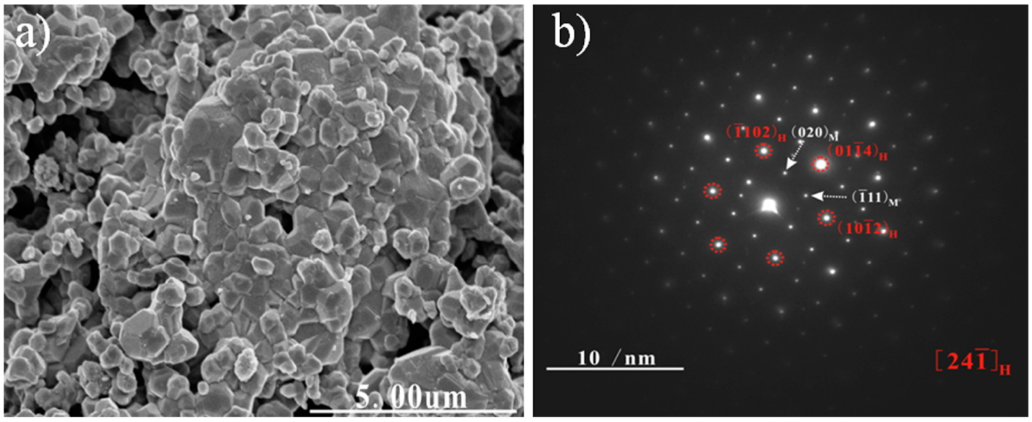

Figure 2. SEM image (a) and SAED pattern (b) of $0.5Li_2MnO_3 \cdot 0.5LiNi_{0.292}Co_{0.375}Mn_{0.333}O_2$.

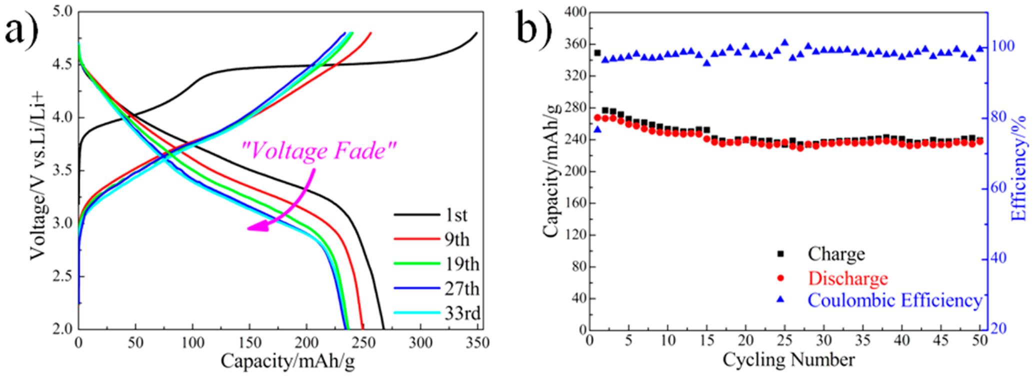

Figure 3. Charge−discharge plots for different cycles (a) and cycling performances (b) of $0.5Li_2MnO_3 \cdot 0.5LiNi_{0.292}Co_{0.375}Mn_{0.333}O_2$.

A simple sketch of the electrolytic cell device is shown in Figure S1. Electrolyte was injected into the device through a tube connected with a small hole on the upper cover before the whole device was sealed by bolt-locking. The tube potential and current of the conventional X-ray generator were set to 40 kV and 25 mA, respectively. Before the test, the cell device stood for 12 h. When the open potential did not change beyond 0.1 mV in 30 min, we began the MPS in situ XRD measurement. We applied a step potential difference $\Delta E = 25$ mV to the as-prepared material to obtain a chronoamperometric curve ($I - t$ curve), and the XRD pattern at each step was observed. One step test lasted for 6000 s. Upward and downward potential steps correspond to the first charge and discharge processes, respectively.

3. RESULTS AND DISCUSSION

3.1. Structural Characterization of $0.5Li_2MnO_3 \cdot 0.5LiNi_{0.292}Co_{0.375}Mn_{0.333}O_2$ Material and Its Electrochemical Performance.

Two sets of XRD patterns of the $0.5Li_2MnO_3 \cdot 0.5LiNi_{0.292}Co_{0.375}Mn_{0.333}O_2$ material are shown in Figure 1. From Figure 1a, the primary diffraction peaks of the observed pattern match well with the peaks of the calculated pattern, which was refined by GSAS based on the α-$NaFeO_2$ structure model, with lattice parameters $c = 14.218$ Å and $a = b = 2.845$ Å. The relatively weak diffraction peaks between 20 and 25°, corresponding to the arrangement of lithium ions in the transition metal (TM) layers, can be indexed to the (020), (110), and $(\bar{1}11)$ diffractions of monoclinic Li_2MnO_3 with $C2/m$ group symmetry, which is shown in Figure 1b.[26] Interestingly, all of the observed peaks in Figure 1a can also be indexed on the basis of the calculated peaks in Figure 1b, which means that this prepared $0.5Li_2MnO_3 \cdot 0.5Li$-

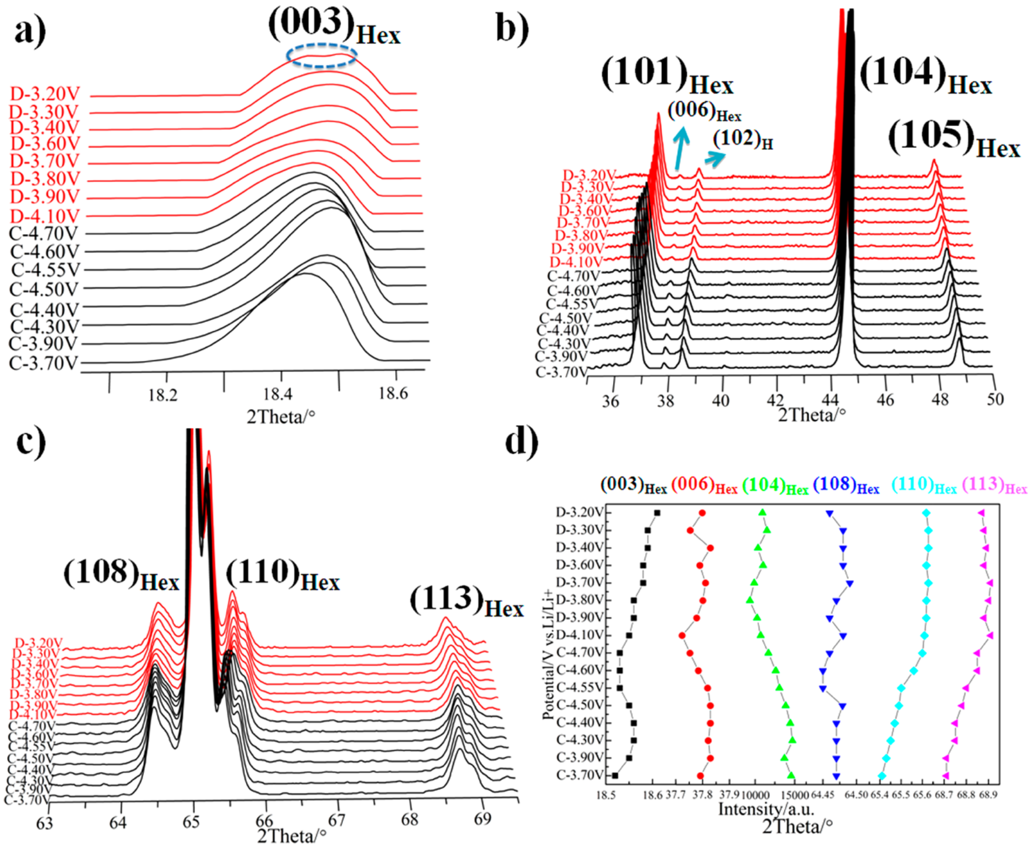

Figure 4. Variations of the in situ XRD patterns at 18.05−18.65° (a), 35.00−50.00° (b), and 63.00−70.00° (c) as well as trend plots of the main diffraction peaks (d) of $0.5Li_2MnO_3{\cdot}0.5LiNi_{0.292}Co_{0.375}Mn_{0.333}O_2$.

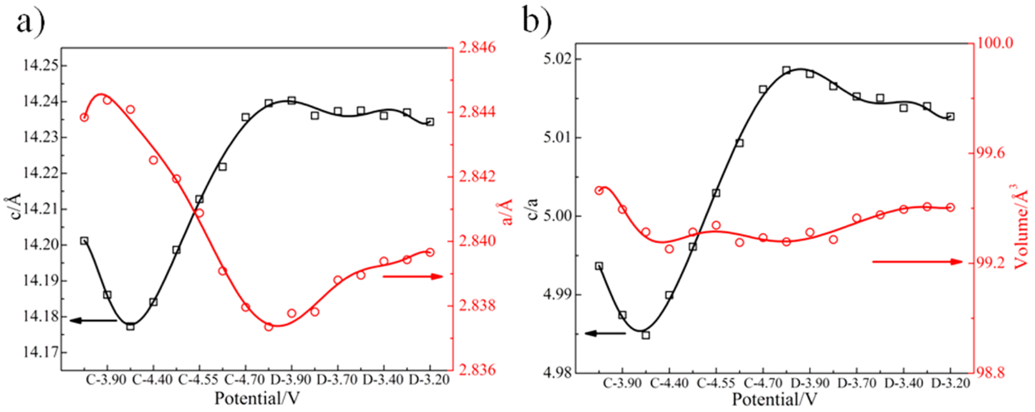

Figure 5. Lattice parameters (a) and layered factors (b) of $0.5Li_2MnO_3{\cdot}0.5LiNi_{0.292}Co_{0.375}Mn_{0.333}O_2$.

$Ni_{0.292}Co_{0.375}Mn_{0.333}O_2$ material is a solid solution with a superlattice structure.[27]

According to the GSAS analysis, the structural host body of the as-prepared material is more similar to layered α-$NaFeO_2$-type $LiMO_2$ ($Rwp_1 < Rwp_2$, $Rp_1 < Rp_2$). The parameters c/a = 4.998 (>4.899), I_{003}/I_{104} = 1.704 (>1.200), $R = (I_{006} + I_{102})/I_{101}$ = 0.272, and Ni_{3a}/Li_{3b} = 2.183% indicate that the crystalline structure of the as-prepared material is well-defined and has a clear layered trait and ordered cation arrangement.[28]

Particles of the as-prepared material are truncated-polyhedral, as shown in Figure 2a, with a mean size of approximately 0.5 μm. Particle size distrubution is shown in Figure S2. The SAED pattern collected along the $[24\bar{1}]$ zone axis is shown in Figure 2b. In the SAED pattern, apart from the fundamental spots (marked by red dash cycles) belonging to the α-$NaFeO_2$-type host structure with space group $R\bar{3}m$, superlattice spots (marked by white arrows) appear. These supperlattice spots can be indexed to the reflections of the monoclinic Li_2MnO_3 component with $C2/m$ group symmetry. The appearance of these superlattice spots, which divide the fundamental hexagonal spots, leads to a 3-fold increase in the distance between oxygen atoms in the α-$NaFeO_2$-type lattice.[29] The presence of these superlattice spots indicates the ordering of lithium ions with TM ions in the TM layers.

As shown in Figure 3a,b, the $0.5Li_2MnO_3{\cdot}0.5LiNi_{0.292}Co_{0.375}Mn_{0.333}O_2$ material delivers a discharge capacity of 267.7 mAh g^{-1} at a current density of 25 mA g^{-1}, with a Coulombic efficiency of 76.7% in the first cycle. The large

Table 1. Refined XRD Parameters and Diffusion Coefficient of the Lithium Ions of $0.5Li_2MnO_3{\cdot}0.5LiNi_{0.292}Co_{0.375}Mn_{0.333}O_2$ under Different Step Potentials

potential (V)	c (Å)	a (Å)	V (Å^3)	c/a	fwhm$_{(003)}$ (deg)	Ni_{3b} (%)	Li_{Oct}–O (Å)[a]	Ni_{Oct}–O (Å)[a]	ln D_{Li+}
C-3.70	14.201	2.844	99.464	4.994	0.201	3.680	2.002	2.042	−19.669
C-3.90	14.186	2.844	99.396	4.987	0.198	3.710	1.999	2.048	−19.903
C-4.30	14.177	2.844	99.314	4.985	0.207	4.089	1.995	2.051	−20.169
C-4.40	14.184	2.843	99.252	4.990	0.204	3.170	2.000	2.045	−20.096
C-4.50	14.199	2.842	99.314	4.996	0.204	2.952	2.001	2.045	−20.782
C-4.55	14.213	2.841	99.338	5.003	0.209	1.890	2.001	2.046	−20.782
C-4.60	14.222	2.839	99.276	5.009	0.231	1.493	2.010	2.036	−20.491
C-4.70	14.236	2.838	99.294	5.016	0.221	0.980	2.008	2.037	−20.754
D-4.10	14.240	2.837	99.278	5.019	0.233	0.897	2.005	2.041	−19.885
D-3.90	14.240	2.838	99.313	5.018	0.263	0.631	2.015	2.031	−20.789
D-3.80	14.236	2.838	99.286	5.016	0.268	0.718	2.013	2.032	−20.662
D-3.70	14.237	2.839	99.364	5.015	0.280	1.338	2.014	2.033	−20.865
D-3.60	14.238	2.839	99.376	5.015	0.275	1.161	2.007	2.040	−20.654
D-3.40	14.236	2.840	99.396	5.014	0.265	1.357	2.022	2.025	−20.911
D-3.30	14.237	2.839	99.406	5.014	0.277	1.412	2.023	2.024	−20.681
D-3.20	14.234	2.840	99.404	5.013	0.274	1.899	2.020	2.027	−21.151

[a] Li_{Oct}–O represents the distance between Li in the octahedral site and its adjacent O^{2-} in Li layers; Ni_{Oct}–O represents the distance between Ni in the octahedral site and its adjacent O^{2-} in TM layers.

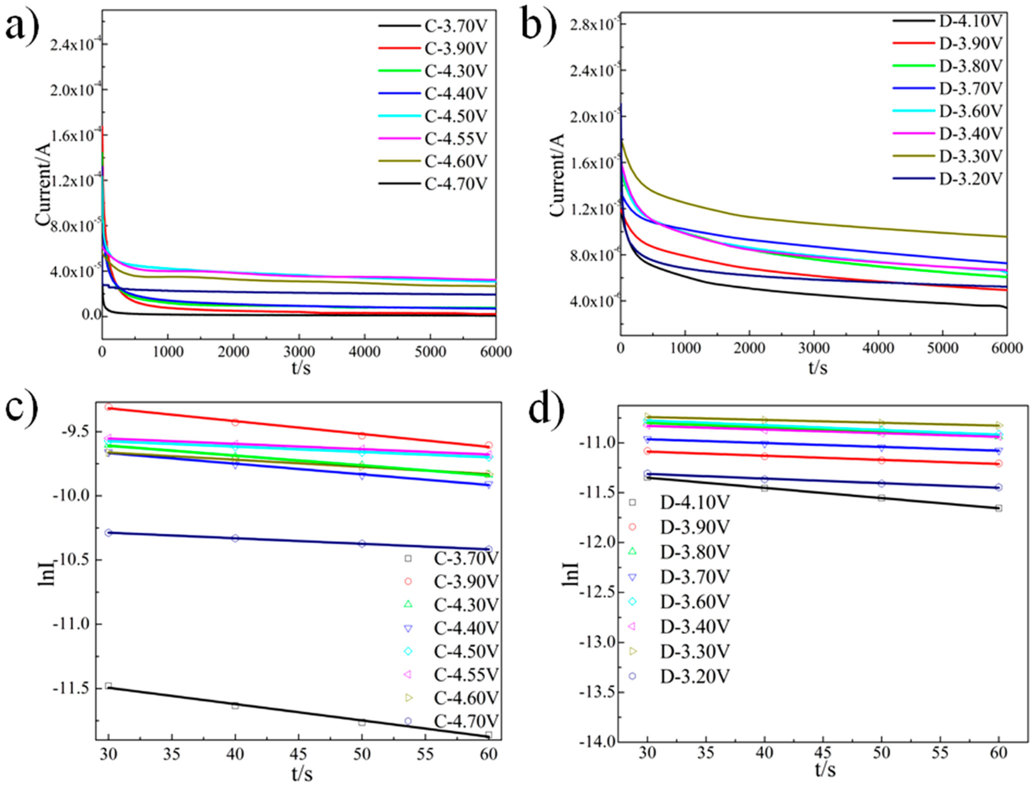

Figure 6. Plots of chronoamperometry at the first charge (a) and discharge (b) processes as well as ln I as a function of t at the first charge (c) and discharge (d) processes of $0.5Li_2MnO_3{\cdot}0.5LiNi_{0.292}Co_{0.375}Mn_{0.333}O_2$.

irreversible capacity loss is attributed to the simultaneous removal of Li^+ and O^{2-} above 4.40 V.[30] The cycling performance of the as-prepared material is good in terms of its capacity retention (88.8% after 50 cycles), whereas the discharge voltage fades slightly. The rate capability of the as-prepared material is moderate when considering the fact that its stable capacity under 1.0 C is as good as 70% of the stable capacity under 1.0 C (shown in Figure S3).

3.2. MPS in Situ XRD. The observed XRD patterns of MPS in situ XRD measurement are shown in Figure 4a–c. From Figure 4d, it can be seen that the (003) diffraction peak shifts toward a higher 2θ angle from 3.70 to 4.30 V during the first charge process, which is attributed to a decrease in the d-spacing of the (003) diffraction peak by the extraction of lithium ions from the $LiMO_2$ component. As shown in Figure 5a, this decrease causes a lattice contraction in the c axis; hence, the c parameter decreases. Meanwhile, the value of the a parameter stabilizes at 8.444 Å, ascribed to a lack of change in the ionic radii with respect to Ni^{2+} or Co^{3+} because oxidation did not occur yet. Above 4.30 V, the position of the (003),

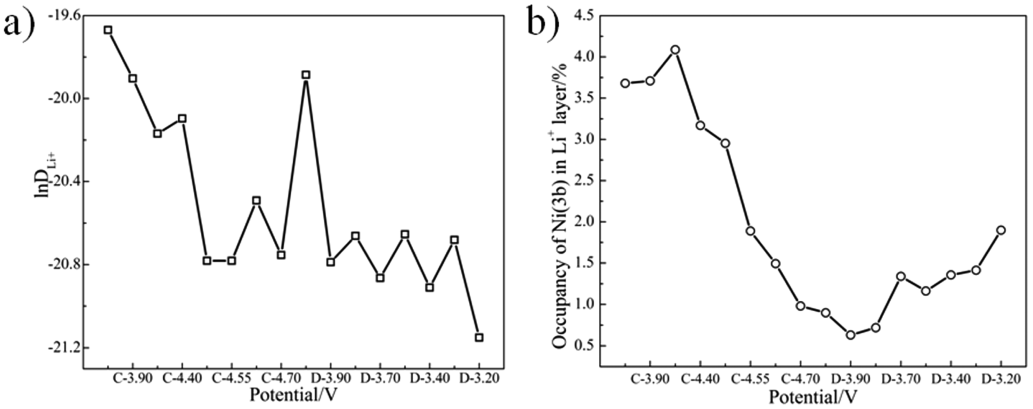

Figure 7. Diffusion coefficient of lithium ions as a function of the step potential (a) and occupancy of Ni in the 3b site of the lithium ion layers (b) of $0.5Li_2MnO_3 \cdot 0.5LiNi_{0.292}Co_{0.375}Mn_{0.333}O_2$.

(006), and (108) diffraction peaks exhibits a clear pathway toward a smaller 2θ angle. On the contrary, the (110), (113), and (102) diffraction peaks shift toward a higher 2θ angle. The variations of these diffraction peak positions indicate that the *c* parameter increases and the *a* parameter decreases. The increase in the *c* parameter means that there is a growing electrostatic repulsive force between O^{2-} ions located in interlayer because of lithium ions extracting from TM layers, whereas the decrease in the *a* parameter indicates a decrease in ionic radii caused by oxidation of Ni^{2+} to Ni^{3+}/Ni^{4+}, which can be proved by the decrease in the distance between Ni in the octahedral site and its adjacent O^{2-} in the TM layers (referred to as Ni_{Oct}—O hereafter; likewise, Li_{Oct}—O will be used to indicate the distance between Li in the octahedral site and its adjacent O^{2-}), as shown in Table 1.[31] Below 3.90 V during the first discharge process, the position of the (003) diffraction peak is completely opposite that of the first charge process, as shown in Figure 4a, which indicates a slight decrease of the *c* parameter in Figure 5a that is associated with a shrinking electrostatic repulsion between O^{2-} caused by Li shielding due to insertion of lithium ions. As for the position of the (110) and (113) diffraction peaks, the trend toward a higher 2θ angle stops, which indicates an increase in the *a* parameter in Figure 5a that corresponds to an increase in the ionic radii resulting from the reduction of Ni^{3+}/Ni^{4+} to Ni^{2+}.[32] In addition, the (104) diffraction peak decreases and increases in its intensity during upward and downward potential steps respectively, which is evidence for the extraction–intercalation of lithium ions in the layered structure.

Remarkably, in addition to a consecutive broadening in the fwhm of the (003) diffraction peak at 4.55 V of the initial charge process, as shown in Table 1, a slight splitting of it at 3.20 V (marked by black dash ellipse) was found during the first discharge process. Moreover, the *c*/*a* ratio shows a large increase with slight changes in the volume of the unit cell during the whole cycle in Figure 5b. Combining the above evidence, we speculate that a lattice distortion within the local domain in the host structure may occur at about 3.20 V during the first discharge process.

The PITT method is based on the evolution of a one-dimensional finite-space diffusion model. Through a particular assumption regarding the diffusion process along with the solution of a partial differential equation to Fick's second law with mathematical manipulation, a computational formula for the lithium ion diffusion coefficient (D_{Li}) was obtained[33]

$$D_{Li} = -\frac{d\ln(I)}{dt} \cdot \frac{4L^2}{\pi^2} \quad (1)$$

D_{Li} is the lithium ion diffusion coefficient, *I* refer to the step current, *t* reflects the step time, and *L* defines the diffusion distance, which is approximated to the cathode thickness that is in common.

The chronoamperometry and ln $I - t$ plots are shown in Figure 6a–d. By combining the slopes of the plots with the thickness of the cathode (L = 8.3 μm, Figure S4), the diffusion coefficient of lithium ions can be calculated through eq 1, and a plot of ln D_{Li+} as a function of the step potential is shown in Figure 7a.

The value of D_{Li+} decreases significantly from 3.70 to 4.30 V during the first charge process, which is attributed to a narrowing in the diffusion path caused by a decrease of both the *c* and *a* parameters, as indicated in Figure 5a. As shown in Figure 5b, the increased occupancy in 3b sites in Li^+ layers by Ni (Ni_{3b}%) between 3.70 and 4.30 V is indicative of the fact that more Ni^{2+} in 3a sites in TM layers has migrated into the octahedral vacancies in the Li^+ layers because some lithium ions have extracted from the octahedral sites and the ionic radius of Li^+ is similar compared to that of Ni^{2+} (0.76 Å for Li^+ and 0.69 Å for Ni^{2+}), which can be confirmed by the increase in Ni_{Oct}—O, as shown in Table 1. From 4.40 to 4.55 V, the lithium ion diffusion process keeps slowing, which may be ascribed to the following factors: (i) disturbance of the growing electrostatic repulsion between oxygen layers caused by the escape of lithium ions from octahedral interstice in Li^+ layers. The evidence for this can be found in Figure 5a and Table 1 with respect to variations in the *c* parameter and Li_{Oct}—O, respectively. The increase in Li_{Oct}—O indicates a weaker atomic binding force between Li and O, and this could lead to removal of a significant number of lithium ions. This extraction causes a growing electrostatic repulsion between oxygen layers, corresponding to the increase in the *c* parameter, as we illustrated previously. Lithium ions could migrate and fill tetrahedral sites adjacent to vacant Li octahedral sites in the TM layer before their extraction,[34] and the growing electrostatic repulsion between oxygen layers could disturb this motion process. (ii) Increasing resistance to Li^+ motion resulted from Ni^{2+} filling the octahedral vacancies in Li^+ layers, which occurred because of migration of Li^+ and TM ions into Li^+ layers and is attributed to oxygen loss in TM layers. The results from Figure 7b and Table 1 demonstration this. Ni in the Li layer could move into the tetrahedral sites that face share

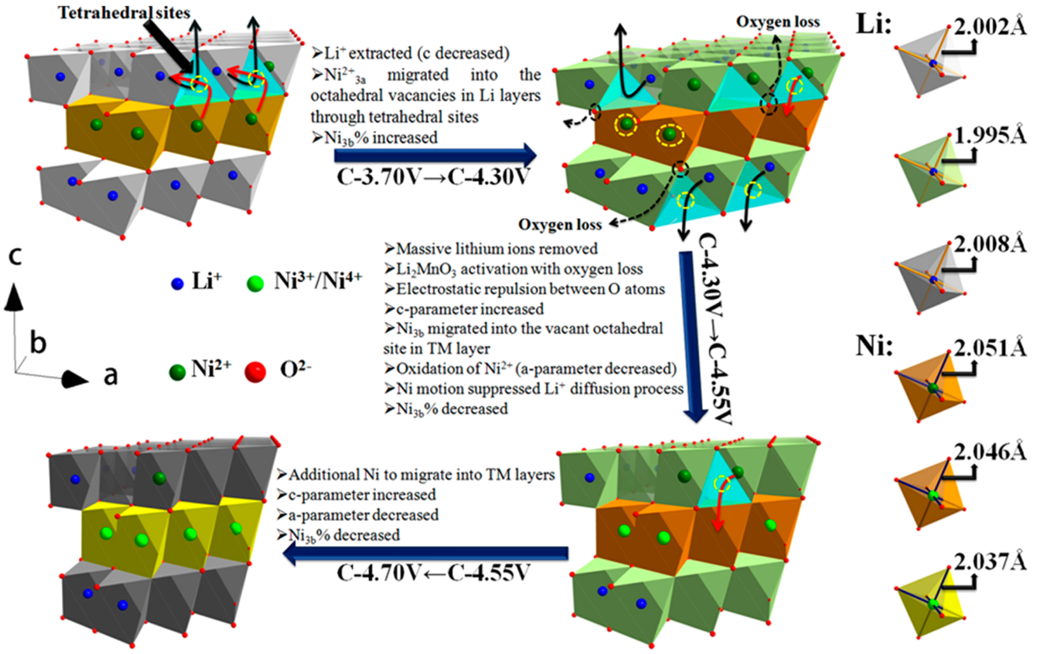

Figure 8. Schematic of the initial charge process of $0.5Li_2MnO_3 \cdot 0.5LiNi_{0.292}Co_{0.375}Mn_{0.333}O_2$.

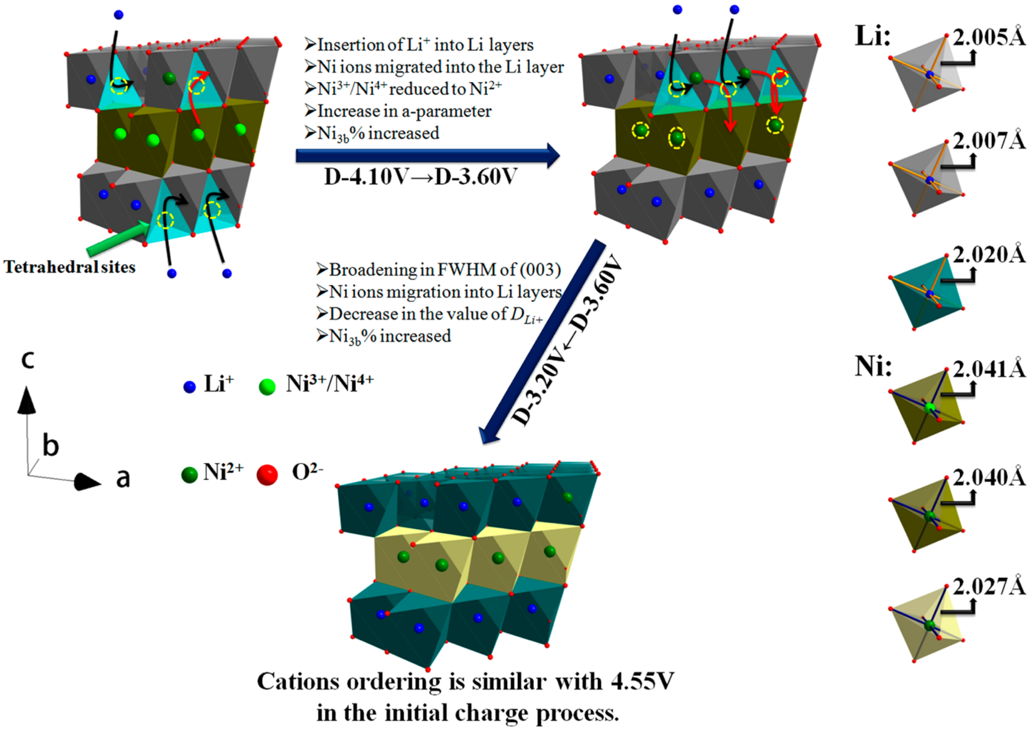

Figure 9. Schematic of the initial discharge process of $0.5Li_2MnO_3 \cdot 0.5LiNi_{0.292}Co_{0.375}Mn_{0.333}O_2$.

with a vacant octahedral site in the TM layer and migrate into the vacant octahedral site in the TM layer upon oxidation, a process that has a low-energy barrier;[35−40] this migration is consistent with the significant decrease in Ni_{3b}% from 3.170 to 1.890%, as shown in Figure 7b. The lithium ion diffusion process could be suppressed by the migration of Ni into vacant octahedral sites in the TM layer,[21] which might be accelerated because oxidation of Ni^{2+} ions in the Li layer to smaller Ni^{3+} or Ni^{4+} ions is not favored relative to those in the TM layer.[41] (iii) Massive energetic consumption used for Li_2MnO_3 activation and corresponding structural changes. The high kinetic barriers associated with concurrent Li^+ extraction, oxygen loss, and structural changes could slow the lithium ion diffusion process.[42] The lithium ion diffusion process is not fast from 4.60 to 4.70 V during the first charge process because of the predominating migration of Ni ions since potentials higher than 4.50 V could induce additional Ni ions to migrate into TM layers.[41] The above-discussed charge process is summarized in Figure 8.

The value of D_{Li+} during the first discharge process is lower than that of the first charge process except for 4.10 V, which is ascribed to the insertion of lithium ions associated with the filling of octahedral vacancies in the Li^+ layers.[43] This insertion results in a drive force that speeds the lithium ion diffusion process. From 3.90 to 3.60 V, Ni ions move out of octahedral sites in the TM layer, occupy adjacent, face-shared tetrahedral sites in the Li layer upon reduction to Ni^{2+}, and migrate into the Li layer,[41] which is consistent with the increase in Ni_{3b}%, as shown in Table 1. Meanwhile, the decrease in Li_{Oct}−O is a sign of a stronger atomic binding force, which makes the Li layers stable. From 3.40 to 3.20 V, the continuous increase in Ni_{3b}% is indicative of Ni ions migrating into Li layers, which corresponds to the trend of a decrease in the value of D_{Li+}. On the basis of the evidence that a slight splitting arises on the (003) peak diffraction and D_{Li+} decreases to a minimum at 3.20 V compared to that during the whole cycle, we speculate that a lattice distortion might occur within the local domain. The above-discussed discharge process is shown in Figure 9.

4. CONCLUSIONS

Li-rich layered oxide $0.5Li_2MnO_3{\cdot}0.5LiNi_{0.292}Co_{0.375}Mn_{0.333}O_2$ material with a solid solution structure was synthesized by an aqueous solution−evaporation route. The as-prepared material delivered a high initial discharge capacity with excellent capacity retention after many cycles. With the aid of MPS in situ XRD measurement, the structural changes and kinetics of the as-prepared material were simultaneously obtained.

During the first charge process, the *c* parameter decreased from 3.70 to 4.30 V, which is attributed to lattice contraction in the *c* axis, and increased from 4.30 to 4.70 V because the O^{2-} electrostatic repulsive force dominated due to the extraction of a significant amount of lithium ions from Li layers (which is attributed to a weaker atomic binding force between Li and O, demonstrated by the increase in Li_{Oct}−O), whereas the *a* parameter underwent a decrease above 4.30 V caused by oxidation of Ni^{2+}, which was proved by the decrease in the value of Ni_{oct}−O. The diffusion of lithium ions kept slowing during the whole initial charge process, which can be mostly attributed to the increasing resistance to Li^+ motion as a result of Ni^{2+} filling the octahedral vacancies in the Li^+ layers (which occurred because of the migration of Li^+ and TM ions into Li^+ layers and because of the high diffusion energy barrier caused by complicated chemical reactions such as Li_2MnO_3 activation and oxygen loss). The Ni_{3b}% results showed that Ni ions in 3a sites in TM layers migrated into the octahedral vacancies in Li^+ layers because some lithium ions extracted from the octahedral sites between 3.70 and 4.30 V; they moved into the tetrahedral sites that face share with a vacant octahedral site in the TM layer and migrated into the vacant octahedral site in the TM layer from 4.30 to 4.70 V during the initial charge process.

During the first discharge process, the value of D_{Li+} increased at 4.10 V because of a powerful drive resulting from the insertion of lithium ions into octahedral vacancies in Li^+ layers. Ni ions moved out of the octahedral sites in the TM layer and migrated into the Li layer as the value of Ni_{3b}% increased from 3.90 to 3.60 V. Below 3.90 V, a slight decrease in the *c* parameter was found due to the shrinking electrostatic repulsion between O^{2-} caused by Li shielding as a result of the insertion of lithium ions. An increase in the *a* parameter was also found, which was due to an increase in the ionic radii because of the reduction of Ni^{3+}/Ni^{4+} to Ni^{2+}. The consecutive broadening in the fwhm of the (003) diffraction peak and the slight splitting of the (003) diffraction peak, along with the value of D_{Li+} decreasing to a minimum at 3.20 V, indicate that a lattice distortion might occur within the local framework.

■ ASSOCIATED CONTENT

Ⓢ Supporting Information

Schematic of the electrolytic cell device for MPS in situ XRD measurement; particle size distribution of the as-prepared material; rate capability of the as-prepared electrode; and cross-section SEM image of the as-prepared electrode slice. This material is available free of charge via the Internet at http://pubs.acs.org.

■ AUTHOR INFORMATION

Corresponding Author

*E-mail: huangl@xmu.edu.cn.

Notes

The authors declare no competing financial interest.

■ ACKNOWLEDGMENTS

This work was supported by the NSFC (grant nos. 21273184 and 21321062), the “863” program (grant no. 2011AA11A254), and SRFDP (20130121110002).

■ REFERENCES

(1) Li, N.; An, R.; Su, Y. F.; Wu, F.; Bao, L. Y.; Chen, L.; Zheng, Y.; Shou, H. F.; Chen, S. The Role of Yttrium Content in Improving Electrochemical Performance of Layered Lithium-Rich Cathode Materials for Li-Ion Batteries. *J. Mater. Chem. A* **2013**, *1*, 9760−9767.

(2) Yu, S. H.; Yoon, T. H.; Mun, J. Y.; Park, S. J.; Kang, Y. S.; Park, J. H.; Oh, S. M.; Sung, Y. E. Continuous Activation of Li_2MnO_3 Component upon Cycling in $Li_{1.167}Ni_{0.233}Co_{0.100}Mn_{0.467}Mo_{0.033}O_2$ Cathode Material for Lithium Ion Batteries. *J. Mater. Chem. A* **2013**, *1*, 2833−2839.

(3) Wu, F.; Li, N.; Su, Y. F.; Lu, H. Q.; Zhang, L. J.; An, R.; Wang, Z.; Bao, L. Y.; Chen, S. Can Surface Modification Be More Effective To Enhance the Electrochemical Performance of Lithium Rich Materials? *J. Mater. Chem.* **2012**, *22*, 1489−1497.

(4) Boulineau, A.; Simonin, L.; Colin, J. F.; Bourbon, C.; Patoux, S. First Evidence of Manganese−Nickel Segregation and Densification upon Cycling in Li-Rich Layered Oxides for Lithium Batteries. *Nano Lett.* **2013**, *13*, 3857−3863.

(5) Gu, M.; Genc, A.; Belharouak, I.; Wang, D. P.; Amine, K.; Thevuthasan, S.; Baer, D. R.; Zhang, J. G.; Browning, N. D.; Liu, J.; Wang, C. M. Nanoscale Phase Separation, Cation Ordering, and Surface Chemistry in Pristine $Li_{1.2}Ni_{0.2}Mn_{0.6}O_2$ for Li-Ion Batteries. *Chem. Mater.* **2013**, *25*, 2319−2326.

(6) Zheng, J. M.; Gu, M.; Xiao, J.; Zuo, P. J.; Wang, C. M.; Zhang, J. G. Corrosion/Fragmentation of Layered Composite Cathode and Related Capacity/Voltage Fading during Cycling Process. *Nano Lett.* **2013**, *13*, 3824−3830.

(7) Wang, J.; He, X.; Paillard, E.; Liu, H. D.; Passerini, S.; Winter, M.; Li, J. Improved Rate Capability of Layered Li-Rich Cathode for Lithium Ion Battery by Electrochemical Treatment. *ECS Electrochem. Lett.* **2013**, *2*, A78−A80.

(8) He, W.; Yuan, D. D.; Qian, J. F.; Ai, X. P.; Yang, H. X.; Cao, Y. L. Enhanced High-Rate Capability and Cycling Stability of Na-Stabilized Layered $Li_{1.2}[Co_{0.13}Ni_{0.13}Mn_{0.54}]O_2$ Cathode Material. *J. Mater. Chem. A* **2013**, *1*, 11397−11403.

(9) Gao, J.; Kim, J.; Manthiram, A. High Capacity $Li[Li_{0.2}Mn_{0.54}Ni_{0.13}Co_{0.13}]O_2−V_2O_5$ Composite Cathodes with Low Irreversible Capacity Loss for Lithium Ion Batteries. *Electrochem. Commun.* **2009**, *11*, 84−86.

(10) Yabuuchi, N.; Yoshii, K.; Myung, S. T.; Nakai, I.; Komaba, S. Detailed Studies of a High-Capacity Electrode Material for Rechargeable Batteries, $Li_2MnO_3−LiCo_{1/3}Ni_{1/3}Mn_{1/3}O_2$. *J. Am. Chem. Soc.* **2011**, *133*, 4404−4419.

(11) Huang, X. L.; Wang, M.; Che, R. C. Modulating the Li^+/Ni^{2+} Replacement and Electrochemical Performance Optimizing of Layered

Lithium-Rich $Li_{1.2}Ni_{0.2}Mn_{0.6}O_2$ by Minor Co Dopant. *J. Mater. Chem. A* **2014**, *2*, 9656−9665.

(12) Liu, J.; Manthiram, A. Functional Surface Modifications of a High Capacity Layered $Li[Li_{0.2}Mn_{0.54}Ni_{0.13}Co_{0.13}]O_2$ Cathode. *J. Mater. Chem.* **2010**, *20*, 3961−3967.

(13) Zhao, Y. J.; Zhao, C. S.; Feng, H. L.; Sun, Z. Q.; Xia, D. G. Enhanced Electrochemical Performance of $Li[Li_{0.2}Ni_{0.2}Mn_{0.6}]O_2$ Modified by Manganese Oxide Coating for Lithium-Ion Batteries. *Electrochem. Solid-State Lett.* **2011**, *14*, A1−A5.

(14) Yu, H. J.; Ishikawa, R.; So, Y. G.; Shibata, N.; Kudo, T.; Zhou, H. S.; Ikuhara, Y. Direct Atomic-Resolution Observation of Two Phases in the $Li_{1.2}Mn_{0.567}Ni_{0.166}Co_{0.067}O_2$ Cathode Material for Lithium-Ion Batteries. *Angew. Chem.* **2013**, *52*, 5969−5973.

(15) Zhao, Y. J.; Ren, W. F.; Wu, R.; Yue, Y. Y.; Sun, Y. C. Improved Molten Salt Synthesis and Structure Evolution upon Cycling of $0.5Li_2MnO_3{\cdot}0.5LiCoO_2$ in Lithium-Ion Batteries. *J. Solid State Electrochem.* **2013**, *17*, 2259−2267.

(16) Oishi, M.; Fujimoto, T.; Takanashi, Y.; Orikasa, Y.; Kawamura, A.; Ina, T.; Yamashige, H.; Takamatsu, D.; Sato, K.; Murayama, H.; Tanida, H.; Arai, H.; Ishii, H.; Yogi, C.; Watanabe, I.; Ohta, T.; Mineshige, A.; Uchimoto, Y.; Ogumi, Z. Charge Compensation Mechanisms in $Li_{1.16}Ni_{0.15}Co_{0.19}Mn_{0.50}O_2$ Positive Electrode Material for Li-Ion Batteries Analyzed by a Combination of Hard and Soft X-ray Absorption Near Edge Structure. *J. Power Sources* **2013**, *222*, 45−51.

(17) Croy, J. R.; Gallagher, K. G.; Balasubramanian, M.; Chen, Z. H.; Ren, Y.; Kim, D. H.; Kang, S. H.; Dees, D. W.; Thackeray, M. M. Examining Hysteresis in Composite $xLi_2MnO_3{\cdot}(1-x)LiMO_2$ Cathode Structures. *J. Phys. Chem. C* **2013**, *117*, 6525−6536.

(18) Gu, M.; Belharouak, I.; Zheng, J. M.; Wu, H. M.; Xiao, J.; Genc, A.; Amine, K.; Thevuthasan, S.; Baer, D. R.; Zhang, J. G.; Browning, N. D.; Liu, J.; Wang, C. M. Formation of the Spinel Phase in the Layered Composite Cathode Used in Li-Ion Batteries. *ACS Nano* **2013**, *7*, 760−767.

(19) Liu, J. L.; Chen, L.; Hou, M. Y.; Wang, F.; Che, R. C.; Xia, Y. Y. General Synthesis of $xLi_2MnO_3{\cdot}(1-x)LiMn_{1/3}Ni_{1/3}Co_{1/3}O_2$ Nanomaterials by a Molten-Salt Method: Towards a High Capacity and High Power Cathode for Rechargeable Lithium Batteries. *J. Mater. Chem.* **2012**, *22*, 25380−25387.

(20) Zhang, H. Z.; Qiao, Q. Q.; Li, G. R.; Gao, X. P. PO_4^{3-} Polyanion-Doping for Stabilizing Li-Rich Layered Oxides as Cathode Materials for Advanced Lithium-Ion Batteries. *J. Mater. Chem. A* **2014**, *2*, 7454−7460.

(21) Mohanty, D.; Kalnaus, S.; Meisner, R. A.; Rhodes, K. J.; Li, J. L.; Payzant, E. A.; Wood, D. L.; Daniel, C. Structural Transformation of a Lithium-Rich $Li_{1.2}Co_{0.1}Mn_{0.55}Ni_{0.15}O_2$ Cathode during High Voltage Cycling Resolved by in Situ X-ray Diffraction. *J. Power Sources* **2013**, *229*, 239−248.

(22) Shen, C. H.; Wang, Q.; Fu, F.; Huang, L.; Lin, Z.; Shen, S. Y.; Su, H.; Zheng, X. M.; Xu, B. B.; Li, J. T.; Sun, S. G. Facile Synthesis of the Li-Rich Layered Oxide $Li_{1.23}Ni_{0.09}Co_{0.12}Mn_{0.56}O_2$ with Superior Lithium Storage Performance and New Insights into Structural Transformation of the Layered Oxide Material during Charge−Discharge Cycle: In Situ XRD Characterization. *ACS Appl. Mater. Interfaces* **2014**, *6*, 5516−5524.

(23) Yu, D. Y. W.; Yanagida, K.; Kato, Y.; Nakamura, H. Electrochemical Activities in Li_2MnO_3. *J. Electrochem. Soc.* **2009**, *156*, A417−A424.

(24) Li, Z.; Fei, D.; Bie, X. F.; Zhang, D.; Cai, Y. M.; Cui, X. R.; Wang, C. Z.; Chen, G.; Wei, Y. J. Electrochemical Kinetics of the $Li[Li_{0.23}Co_{0.3}Mn_{0.47}]O_2$ Cathode Material Studied by GITT and EIS. *J. Phys. Chem. C* **2010**, *114*, 22751−22757.

(25) Amalraj, F.; Talianker, M.; Markovsky, B.; Sharon, D.; Burlaka, L.; Shafir, G.; Zinigrad, E.; Haik, O.; Aurbach, D.; Lampert, J.; Dobrick, M. S.; Garsuch, A. Study of the Lithium-Rich Integrated Compound $xLi_2MnO_3{\cdot}(1-x)LiMO_2$ (x around 0.5; M = Mn, Ni, Co; 2:2:1) and Its Electrochemical Activity as Positive Electrode in Lithium Cells. *J. Electrochem. Soc.* **2012**, *160*, A324−A337.

(26) Lei, C. H.; Bareño, J.; Wen, J. G.; Petrov, I.; Kang, S. H.; Abraham, D. P. Local Structure and Composition Studies of $Li_{1.2}Ni_{0.2}Mn_{0.6}O_2$ by Analytical Electron Microscopy. *J. Power Sources* **2008**, *178*, 422−433.

(27) Jarvis, K. A.; Deng, Z. Q.; Allard, L. F.; Manthiram, A.; Ferreira, P. J. Atomic Structure of a Lithium-Rich Layered Oxide Material for Lithium-Ion Batteries: Evidence of a Solid Solution. *Chem. Mater.* **2011**, *23*, 3614−3621.

(28) Zhang, X. Y.; Jiang, W. J.; Mauger, A.; Qi, L.; Gendron, F.; Julien, C. M. Minimization of the Cation Mixing in $Li_{1+x}(NMC)_{1-x}O_2$ as Cathode Material. *J. Power Sources* **2010**, *195*, 1292−1301.

(29) Bareño, J.; Balasubramanian, M.; Kang, S. H.; Wen, J. G.; Lei, C. H.; Pol, S. V.; Petrov, I.; Abraham, D. P. Long-Range and Local Structure in the Layered Oxide $Li_{1.2}Co_{0.4}Mn_{0.4}O_2$. *Chem. Mater.* **2011**, *23*, 2039−2050.

(30) Wang, J.; Yuan, G. X.; Zhang, M. H.; Qiu, B.; Xia, Y. G.; Liu, Z. P. The Structure, Morphology, and Electrochemical Properties of $Li_{1+x}Ni_{1/6}Co_{1/6}Mn_{4/6}O_{2.25+x/2}$ ($0.1 \leq x \leq 0.7$) Cathode Materials. *Electrochim. Acta* **2012**, *66*, 61−66.

(31) Yang, X. Q.; Sun, X.; McBreen, J. New Findings on the Phase Transitions in $Li_{1-x}NiO_2$: In Situ Synchrotron X-ray Diffraction Studies. *Electrochem. Commun.* **1999**, *1*, 227−232.

(32) Liao, P. Y.; Duh, J. G.; Lee, J. F.; Sheu, H. S. Structural Investigation of $Li_{1-x}Ni_{0.5}Co_{0.25}Mn_{0.25}O_2$ by in Situ XAS and XRD Measurements. *Electrochim. Acta* **2007**, *53*, 1850−1857.

(33) Rho, Y. H.; Kanamura, K. Li^+ Ion Diffusion in $Li_4Ti_5O_{12}$ Thin Film Electrode Prepared by PVP Sol−Gel Method. *J. Solid State Chem.* **2004**, *177*, 2094−2100.

(34) Kobayashi, H.; Arachi, Y.; Kageyama, H.; Tatsumi, K. Structural Determination of $Li_{1-y}Ni_{0.5}Mn_{0.5}O_2$ ($y = 0.5$) Using a Combination of Rietveld Analysis and the Maximum Entropy Method. *J. Mater. Chem.* **2004**, *14*, 40−42.

(35) Breger, J.; Meng, Y. S.; Hinuma, Y.; Kumar, S.; Kang, K. S.; Yang, S. H.; Ceder, G.; Grey, C. P. Effect of High Voltage on the Structure and Electrochemistry of $LiNi_{0.5}Mn_{0.5}O_2$: A Joint Experimental and Theoretical Study. *Chem. Mater.* **2006**, *18*, 4168−4181.

(36) Reed, J.; Ceder, G. Role of Electronic Structure in the Susceptibility of Metastable Transition-Metal Oxide Structures to Transformation. *Chem. Rev.* **2004**, *104*, 4513−4533.

(37) Ma, X. H.; Kang, K. S.; Ceder, G.; Meng, Y. S. Synthesis and Electrochemical Properties of Layered $LiNi_{2/3}Sb_{1/3}O_2$. *J. Power Sources* **2007**, *173*, 550−555.

(38) Kim, Y.; Kim, D.; Kang, S. Experimental and First-Principles Thermodynamic Study of the Formation and Effects of Vacancies in Layered Lithium Nickel Cobalt Oxides. *Chem. Mater.* **2011**, *23*, 5388−5397.

(39) Luo, G. X.; Zhao, J. J.; Ke, X. Z.; Zhang, P. B.; Sun, H. Q.; Wang, B. L. Structure, Electrode Voltage and Activation Energy of $LiMn_xCo_yNi_{1-x-y}O_2$ Solid Solutions as Cathode Materials for Li Batteries from First-Principles. *J. Electrochem. Soc.* **2012**, *159*, A1203−A1208.

(40) Xu, B.; Fell, C. R.; Chi, M.; Meng, Y. S. Identifying Surface Structural Changes in Layered Li-Excess Nickel Manganese Oxides in High Voltage Lithium Ion Batteries: A Joint Experimental and Theoretical Study Energy. *Environ. Sci.* **2011**, *4*, 2223−2233.

(41) Li, H. H.; Yabuuchi, N.; Meng, Y. S.; Kumar, S.; Breger, J.; Grey, C. P.; Yang, S. H. Changes in the Cation Ordering of Layered O3 $Li_xNi_{0.5}Mn_{0.5}O_2$ during Electrochemical Cycling to High Voltages: An Electron Diffraction Study. *Chem. Mater.* **2007**, *19*, 2551−2565.

(42) Wang, Y. H.; Bie, X. F.; Nikolowski, K.; Ehrenberg, H.; Du, F.; Hinterstein, M.; Wang, C. Z.; Chen, G.; Wei, Y. J. Relationships between Structural Changes and Electrochemical Kinetics of Li-Excess $Li_{1.13}Ni_{0.3}Mn_{0.57}O_2$ during the First Charge. *J. Phys. Chem. C* **2013**, *117*, 3279−3286.

(43) Johnson, C. S.; Li, N. C.; Lefief, C.; Vaughey, J. T.; Thackeray, M. M. Synthesis, Characterization and Electrochemistry of Lithium Battery Electrodes: $xLi_2MnO_3{\cdot}(1-x)LiMn_{0.333}Ni_{0.333}Co_{0.333}O_2$ ($0 \leq x \leq 0.7$). *Chem. Mater.* **2008**, *20*, 6095−6106.